(This is a sample cover image for this issue. The actual cover is not yet available at this time.)

Earth and Planetary Science Letters 333–334 (2012) 304–316

Contents lists available at SciVerse ScienceDirect

Earth and Planetary Science Letters

journal homepage: www.elsevier.com/locate/epsl

Magnesium isotope fractionation during precipitation of inorganic calcite under laboratory conditions

Weiqiang Li [a,c,*], Suvankar Chakraborty [b,c], Brian L. Beard [a,c], Christopher S. Romanek [b,c], Clark M. Johnson [a,c]

[a] University of Wisconsin-Madison, Department of Geoscience, 1215 West Dayton Street, Madison, WI 53706, USA
[b] Department of Earth and Environmental Sciences, University of Kentucky, Lexington, KY 40506, USA
[c] NASA Astrobiology Institute, USA

ARTICLE INFO

Article history:
Received 18 November 2011
Received in revised form
29 March 2012
Accepted 6 April 2012
Editor: G. Henderson

Keywords:
Mg isotope
Mg-calcite
carbonate
isotope fractionation
free-drift experiment
vital effect

ABSTRACT

The Mg isotope composition of biogenic and inorganic carbonate bears on paleoclimate and paleooceanography studies because of the potential for constraining temperatures, so-called "vital" effects, and marine Mg fluxes. Previous work has shown that marine organisms produce a wide range of Mg isotope compositions that are species dependent, where $\Delta^{26/24}Mg_{carb\text{-}sol}$ fractionations vary from −1‰ to −5‰ (e.g., Hippler et al., 2009, GCA). Constraining Mg isotope fractionation during inorganic carbonate precipitation is important because this serves as a baseline with which to compare biogenic samples, as well as constrain Mg cycling in natural environments. We report Mg isotope fractionation factors between Mg-bearing calcite and aqueous Mg (Mg/Ca molar ratio between 3:1 and 13:1) from 20 free-drift and one chemo-stat experiment conducted at temperatures between 4 °C and 45 °C, for solutions buffered at P_{CO_2} between 0.038% and 3%. Pure $CaCO_3$ seed crystals were used to promote the heterogeneous growth of carbonate from solution, and to minimize kinetic isotope effects associated with nucleation and rapid precipitation from strongly super-saturated solutions. Under these conditions, calcite overgrowths that contained 0.8–14.9 mol% $MgCO_3$ precipitated on the seed crystals. The measured $^{26}Mg/^{24}Mg$ fractionation factors between Mg-calcite and solution ($\Delta^{26}Mg_{cal\text{-}sol}$) are modestly correlated with temperature, changing from −2.70‰ at 4 °C to −2.22‰ at 45 °C. The fractionation factors are not correlated with experimental conditions (chemo-stat vs. free drift), Mg content of the overgrowth, P_{CO_2}, or the Mg/Ca ratio of the solution. The temperature-dependence of the Mg isotope fractionation is: $\Delta^{26}Mg_{cal\text{-}sol} = (-0.158 \pm 0.051) \times 10^6/T^2 - (0.74 \pm 0.56)$, where T is temperature in Kelvin. Fractionation of Mg isotopes in calcite is much less sensitive to temperature than oxygen isotope fractionation, which limits its application as a geothermometer. In contrast, the Mg isotope fractionations for biogenically precipitated Mg calcite vary greatly, suggesting its potential to discern "vital" effects in natural samples. Finally, the relatively small temperature effect on Mg isotope fractionation greatly simplifies use of Mg isotopes in modern or ancient marine systems to constrain Mg fluxes, including continental weathering.

1. Introduction

Carbonates provide important records for a variety of sedimentological, environmental, and biological processes. Abiogenic carbonates such as speleothems and biogenic marine carbonates are widely studied as archives of paleo-environmental conditions (e.g., Lea, 2003; Wang et al., 2001). The oxygen isotope composition of biogenic marine carbonates has long been used to infer paleo-climate (e.g., Emiliani, 1955; Hays et al., 1976), and more recent studies have used carbon isotopes and trace-element concentrations from carbonate minerals as paleo-climate proxies (e.g., Fairchild and Treble, 2009; Lea, 2003; McDermott, 2004). Additionally, workers have investigated the utility of Ca isotopes as paleo-climate proxies where, for example, significant $\delta^{44/40}Ca$ variation in marine carbonate in the last 500 Ma has been interpreted to reflect changes in global Ca cycling (e.g., De La Rocha and DePaolo, 2000; Farkas et al., 2007a; 2007b; Heuser et al., 2005). Magnesium is a minor element in many carbonates and its isotopic composition has been evaluated for its usefulness as a paleo-climate proxy in both marine and terrestrial environments (e.g., Buhl et al., 2007; Eisenhauer et al., 2009; Hippler et al., 2009).

Ample field studies have suggested significant Mg isotope fractionation between carbonate and aqueous solution. Relative to carbonates, igneous rocks have generally limited variation in Mg isotope composition, indicating that at high-temperature Mg

* Corresponding author at: University of Wisconsin-Madison, Department of Geoscience, 1215 West Dayton Street, Madison, WI 53706, USA.
Tel.: +1 6087727386.
E-mail address: liweiq@gmail.com (W. Li).

0012-821X/$ - see front matter © 2012 Elsevier B.V. All rights reserved.
http://dx.doi.org/10.1016/j.epsl.2012.04.010

is restricted in its isotopic composition (Fig. 1; e.g., Chakrabarti and Jacobsen, 2010; Dauphas et al., 2010; Handler et al., 2009; Li et al., 2010; Liu et al., 2010; Shen et al., 2009; Teng et al., 2010, 2007; Yang et al., 2009). In contrast, δ^{26}Mg values of low-temperature components of the Mg cycle, such as riverine inputs, range from −3.84‰ to 0.75‰, reflecting isotopic fractionation during weathering, and variation of catchments, particularly in the proportions of carbonate to silicate rock (e.g., Brenot et al., 2008; de Villiers et al., 2005; Pogge von Strandmann et al., 2008a, 2008b; Tipper et al., 2006a, 2008, 2006b; Wimpenny et al., 2011). The weighted average δ^{26}Mg value of modern riverine input to the oceans is estimated at −1.09‰ (Tipper et al., 2006b), distinct from the homogeneous δ^{26}Mg value of ca. −0.8‰ for modern ocean seawater (Fig. 1). This contrast is attributed to precipitation of marine carbonate that has low δ^{26}Mg values ranging from −5.3‰ to −1‰ (Fig. 1; Brenot et al., 2008; Buhl et al., 2007; Chang et al., 2003; de Villiers et al., 2005; Galy et al., 2002; Hippler et al., 2009; Immenhauser et al., 2010; Jacobson et al., 2010; Tipper et al., 2006a, 2006b).

Previous investigations of different marine organisms of known habitat demonstrate that fractionation in ^{26}Mg/^{24}Mg ratios during growth of carbonate skeletons in marine organisms range from ca. −5‰ to −1‰, and are species-dependent (Chang et al., 2004; Hippler et al., 2009; Müller et al., 2011; Pogge von Strandmann, 2008; Wombacher et al., 2006). In contrast, Mg isotope fractionation during abiogenic precipitation of carbonate is relatively little studied. Galy et al. (2002) inferred the ^{26}Mg/^{24}Mg fractionation between carbonate and solution to be −2.80‰ to −2.57‰ at temperatures of 4–17 °C, based on analysis of speleothem samples and drip water from caves, and they suggested that the variation in fractionation was at most 0.04‰/°C. Immenhauser et al. (2010) reported carbonate-solution ^{26}Mg/^{24}Mg fractionations of −2.3‰ to −1.6‰ for laboratory calcite precipitation experiments at 10.3 °C. Finally, isotopic fractionations have been reported in abstracts for two laboratory experiments where carbonate was precipitated at 25 °C (−2.4 ± 0.2‰, Kisakurek et al., 2009 and −2.2 ± 0.2‰, Saulnier et al., 2011).

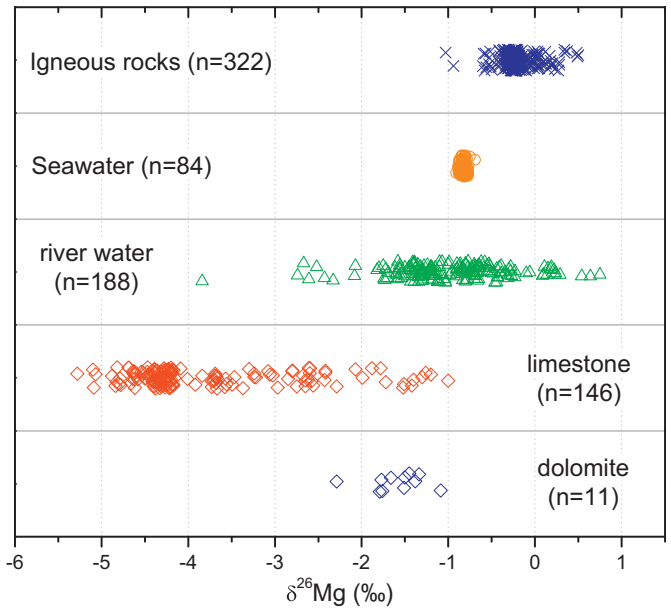

Fig. 1. Compilation of published Mg isotope data from different geological reservoirs. δ^{26}Mg values of igneous rocks are from Tipper et al. (2006a, 2008); Teng et al. (2007, 2010), Wiechert and Halliday (2007), Brenot et al. (2008), Chakrabarti and Jacobsen (2010), Dauphas et al. (2010), Jacobson et al. (2010), Li et al. (2010) and Liu et al. (2010); δ^{26}Mg values of seawater are from de Villiers et al. (2005), Tipper et al. (2006a, 2008, 2010), Hippler et al. (2009), Teng et al. (2010) and Ling et al., (2011); δ^{26}Mg values of river water are from de Villiers et al. (2005), Tipper et al. (2006a, 2006b), Brenot et al. (2008), Pogge von Strandmann et al. (2008a, b) and Wimpenny et al (2011); δ^{26}Mg values of limestone (Mg-calcite) are from Galy et al. (2002), de Villiers et al. (2005), Tipper et al. (2006a), Buhl et al. (2007), Brenot et al. (2008), Hippler et al. (2009) and Immenhauser et al. (2010); δ^{26}Mg values of dolomite are from Galy et al. (2002), Chang et al. (2003), Brenot et al. (2008), and Jacobson et al. (2010).

In this study, we investigated Mg isotope fractionation between carbonate and aqueous Mg solutions from 4 °C to 45 °C under various P_{CO_2} and aqueous Mg–Ca concentrations. Understanding the controls on Mg isotope fractionation during inorganic calcite precipitation is important to interpret the variable Mg isotope data measured from carbonates in nature. Experimental determination of isotopic fractionation between aqueous solution and carbonate using classical precipitation methods may be complicated by kinetic effects because initiation of precipitation generally requires solutions that are highly supersaturated to overcome nucleation energy barriers (Mullin, 2001). Once nucleation is initiated, very rapid mineral precipitation follows, which in turn can produce kinetic isotope fractionations that reflect non-equilibrium isotope transport to the crystal surface (e.g., Lemarchand et al., 2004). Kinetic isotope fractionations are commonly observed in carbonate precipitation experiments and have been discussed for Mg (Immenhauser et al., 2010), Ca (e.g., Lemarchand et al., 2004), O and C (e.g., Kim and O'Neil, 1997; Romanek et al., 1992) in calcite. Common experimental strategies for assessing kinetic isotope effects include varying the precipitation rate, where equilibrium isotope fractionation may be inferred by extrapolation to zero precipitation rates, or if measured fractionations are invariant with respect to precipitation rate (e.g., Lemarchand et al., 2004; Li et al., 2011). Here we attempt to circumvent kinetic Mg isotope fractionation through use of Mg-free calcite seed crystals (Romanek et al., 1992), which strongly reduces or eliminates nucleation energy barriers, allowing carbonate precipitation from solutions that are not strongly supersaturated (Mullin, 2001). Such an approach may more closely approximate equilibrium isotope fractionation than approaches that use homogeneous nucleation from super-saturated solutions.

2. Experimental methods

2.1. Isotope analysis

2.1.1. Instrumentation and data reporting

Magnesium isotope measurements were made at the University of Wisconsin-Madison, using a Micromass *IsoProbe* MC-ICP-MS. Helium was used as the collision gas for thermalization and H_2 was used as a reactive gas to minimize isobaric interferences at masses 25 and 26, which are thought to be $H^{12}C_2$ and $^{12}C^{14}N$, respectively. Magnesium solutions were introduced into the Ar plasma using a self-aspirating 50 or 100 μL/min nebulizer coupled with a Cetac *Aridus II* membrane desolvating system. The cone voltage was set to 20–50 V. These conditions produce a total Mg ion intensity of 4–8 × 10^{-11} A using a 3 ppm Mg solution. Washout between samples used a 2% HNO_3 solution for 6 min. Overall, the "on-peak" blank acid produced a typical ion intensity of 5.5 × 10^{-15}, −5.7 × 10^{-16}, and 4.3 × 10^{-16} A at masses 24, 25, and 26, respectively, and these did not change during an analytical session.

Magnesium isotope ratios were determined using a standard-sample-standard bracketing technique using an in-house Mg standard (HPS909104, Table 1) as the bracketing standard. Samples were typically diluted to 3 ppm ± 5%. Matrix effects associated with Mg concentration were corrected by analysis of the standard solution diluted over a range of 1.5–4.5 ppm Mg, following methods discussed by Albarède and Beard (2004), which typically resulted in a correction of less than ± 0.03‰ in the ^{26}Mg/^{24}Mg ratio for the samples. Isotopic ratios were

Table 1
Mg isotope compositions and external precisions of standards and test solutions passed through ion-exchange chromatography. Analyses were made using HPS909104 as the in-house Mg isotope standard, and data are reported relative to DSM3.

Sample	δ^{26}Mg	2 SD	δ^{25}Mg	2 SD	*n*
Isotope standards (Isoprobe with Aridus)					
DSM3	0.02	0.13	0.00	0.09	109
Cambridge1	−2.57	0.12	−1.33	0.10	87
NBS980	−4.09	0.09	−2.10	0.09	13
HPS909104[a]	−0.67	0.13	−0.34	0.08	49
HPS932001[a]	−2.90	0.13	−1.50	0.08	48
Isotope composition of Cambridge1 in reference (selected)					
Cambridge1 (Galy et al., 2003)	−2.58	0.14	−1.33	0.07	35
Cambridge1 (Tipper et al., 2006a, 2006b)	−2.60	0.14	−1.34	0.08	168
Cambridge1 (Pearson et al., 2006)	−2.57	0.13	−1.34	0.04	69
Cambridge1 (Hippler et al., 2009)	−2.58	0.04	−1.34	0.02	56
Cambridge1 (Huang et al., 2009)	−2.63	0.11	−1.36	0.07	44
Cambridge1 (Isoprobe with spray chamber, Li et al., 2011)	−2.57	0.15	−1.32	0.09	48
Test solutions processed through the complete four-stage column chemistry					
50 μg HPS909104	−0.79	0.16	−0.48	0.14	1
100 μg HPS909104	−0.68	0.16	−0.37	0.15	4
HMC (50 μg Mg equv.)[b]	−0.68	0.20	−0.37	0.12	7
LMC-A (50 μg Mg equv.)[c]	−0.71	0.16	−0.40	0.07	10
LMC-B (50 μg Mg equv.)[d]	−0.61	0.13	−0.30	0.05	4
All test solutions	**−0.69**	**0.17**	**−0.38**	**0.10**	**26**
Hawaiian seawater[e]	−0.87	0.02	−0.45	0.02	2

In this study, the test solutions were dispersed between samples during the column chemistry.

[a] HPS909104 and HPS932001 are pure Mg stock solutions purchased from High-Purity Standards, Inc.
[b] HMC test solution contains 50 ppm Mg (HPS909104) and 720 ppm Ca.
[c] LMC-A test solution contains 50 ppm Mg (HPS909104) and 3920 ppm Ca.
[d] LMC-B test solution contains 50 ppm Mg (HPS909104), 3920 Ca, 50 ppm Na, 50 ppm Al, 50 ppm Mn, and 50 ppm Fe.
[e] Seawater was treated twice with step 3 during column chemistry for complete removal of Na.

calculated by subtracting on-peak zeros obtained using a 60 s on-peak acid blank measurement prior to forty 10 s on-peak integrations of the analyte solution. This measurement routine results in a typical internal (2 standard error) precision of better than ±0.04‰ for ^{26}Mg/^{24}Mg and ±0.02‰ for ^{25}Mg/^{24}Mg.

Magnesium isotope compositions are reported using the standard per mil (‰) notation of δ^{26}Mg for the ^{26}Mg/^{24}Mg isotope ratios, where

$$\delta^{26}\mathrm{Mg} = [(^{26}\mathrm{Mg}/^{24}\mathrm{Mg}_{\mathrm{sample}})/(^{26}\mathrm{Mg}/^{24}\mathrm{Mg}_{\mathrm{DSM3}}) - 1] \times 1000 \quad (1)$$

DSM3 is the international Mg isotope standard (Galy et al., 2003). δ^{25}Mg values for the ^{25}Mg/^{24}Mg isotope ratios are reported using a similar formulation. Fractionation in Mg isotopes between two phases A and B is expressed as

$$\Delta^{26}\mathrm{Mg}_{\mathrm{A-B}} = \delta^{26}\mathrm{Mg}_{\mathrm{A}} - \delta^{26}\mathrm{Mg}_{\mathrm{B}} \approx 10^3 \ln \alpha^{26/24}_{\mathrm{A-B}} \quad (2)$$

The error in Mg isotope fractionation factors is calculated by the error propagation function:

$$\mathrm{Err}\Delta\mathrm{Mg}_{\mathrm{A-B}} = [(\mathrm{Err}\delta\mathrm{Mg}_{\mathrm{A}})^2 + (\mathrm{Err}\delta\mathrm{Mg}_{\mathrm{B}})^2]^{1/2} \quad (3)$$

where $\mathrm{Err}\Delta\mathrm{Mg}_{\mathrm{A-B}}$ is the error of the Mg isotope fractionation factor between phases A and B, and $\mathrm{Err}\delta\mathrm{Mg}_{\mathrm{A}}$ and $\mathrm{Err}\delta\mathrm{Mg}_{\mathrm{B}}$ are the errors of measurements of isotope composition of phases A and B, respectively.

Note in the right side of Eq. (2), the isotopic fractionation factor ($\alpha^{26/24}_{\mathrm{A-B}}$) may be related to the reduced partition function ratio (RPFR) for ^{26}Mg/^{24}Mg (β) for phases A and B via:

$$\alpha^{26/24}{}_{\mathrm{A-B}} = \beta_{\mathrm{A}}/\beta_{\mathrm{B}} \quad (4)$$

where β_{A} (or β_{B}) is the RPFR for A (or B), referenced to an ideal gas of Mg atoms. The β factors for individual phases can be calculated, for example, using quantum-mechanical methods (Rustad et al., 2010; Schauble, 2004, 2011). The equilibrium isotope fractionation factors between A and B therefore can be derived using Eq. (4) if their β factors are known. Combination of Eq. (2) and Eq. (4) enables comparison of calculated and experimentally determined isotope fractionation factors.

2.1.2. Column chemistry

Approximately 50 mg of Mg–Ca solution or 10 mg of carbonate was processed through an ion-exchange chromatographic procedure to purify Mg from other cations while obtaining quantitative Mg yields. Samples were initially converted to chloride form by repeated dissolution and evaporation in HCl, followed by a four-stage purification process. Stage 1 separated Ca and Mg using 3 mL of Biorad AG-MP-50 cation exchange resin in 2.2 M HCl, and carbonate samples were processed twice through this stage because of the high Ca/Mg ratio of the samples. Stage 2 removed Mn using 0.3 mL of AG-MP-50 resin, eluted with a mixture of 93% acetone and 7% 0.5 M HCl. Stage 3 removed Na, Al, Ti and Fe using 0.3 mL of AG-50W-X8 200–400 mesh cation exchange resin, with 0.5 M, 1 M, and 1.5 M HNO_3. A final stage removed any last vestiges of Ca using 0.3 mL Eichrom DGA resin in 2 M HNO_3. The details of each column procedure are provided in Appendix 1. In general, concentrations of matrix elements such as Ca, Mn, Fe, Na, Al were less than 1% of Mg after the four-stage column treatment, and tests showed that the matrix effect caused by these impurities was not discernable in instrumental mass bias. Recovery of Mg for the total procedure was 96 ± 4% (1σ, n=22), as determined by MC-ICP-MS analysis of test solutions that were treated as samples. We note that the slightly less than 100% recovery may be caused by Mg loss during pipetting and drying down steps, and does not reflect loss on the columns. This conclusion is supported by the recovery of original Mg isotope compositions for test solutions, as discussed below. Isotope dilution analysis using a ^{26}Mg spike indicates that the eluent cut before the Mg cut in step 3 of the procedure contains 0.6–1.6 ng Mg (n=4), which is negligible compared with the ~100 μg Mg that was loaded. Total procedural blanks were also determined using isotope dilution and found to be negligible (5.6–6.9 ng Mg, n=2).

2.1.3. Precision and accuracy

The long-term external precision of Mg isotope analysis, determined by repeat analysis of international Mg isotope standards against an in-house stock solution over 8 months, is better than 0.13‰ for $^{26}Mg/^{24}Mg$ and 0.09‰ for $^{25}Mg/^{24}Mg$ ($n=109$, 2 standard deviation or 2 SD, Table 1), and is comparable with that of the wet-plasma method as reported by Li et al. (2011). The accuracy of the total analytical procedure was monitored by analyses of pure in-house Mg standards and test solutions that were processed along with samples using the four-stage column procedure described above. The test solutions were made from in-house Mg standards and other matrix elements (e.g., Ca) to mimic high-Mg calcite (Ca/Mg=9:1, molar ratio) and low-Mg calcite (Ca/Mg=49:1, molar ratio). The measured isotope compositions of the test solutions match that of the in-house standard, with a reproducibility better than 0.17‰ for $^{26}Mg/^{24}Mg$ and 0.10‰ for $^{25}Mg/^{24}Mg$ (2 SD, $n=26$, Table 1). As an additional check on accuracy, Hawaiian seawater was analyzed with this procedure and the Mg isotope results ($\delta^{26}Mg=-0.87\pm0.02$‰, $n=2$, Table 1) are consistent with seawater values reported by other studies (e.g., Ling et al., 2011; Tipper et al., 2006b), which further validates the analytical methods in this study.

2.2. Synthesis experiments of Mg-bearing carbonate

2.2.1. Reagents and analytical methods

Synthesis of inorganic carbonates was carried out at the University of Kentucky. Experimental solutions were prepared by mixing different aliquots of stock solutions of $MgCl_2\cdot6H_2O$, $CaCl_2\cdot2H_2O$, and $NaHCO_3$ that were pre-equilibrated with pure $CO_{2(g)}$. Most experiments were run as "free-drift" experiments while one experiment was run as "chemo-stat" (described below). The Mg isotope compositions of the initial solutions were identical in all experiments.

The concentrations of Mg and Ca in the solutions at the beginning and end of an experiment were determined by ICP-MS with accuracy better than 6%. The total alkalinity of each solution was determined by autotitration (905 Titrando) with NIST-traceable certified titrants to better than 0.1%. The pH of each solution was measured using an ORION pH meter. The pH electrode (Cole-Parmer) was calibrated with NIST-traceable standard buffer solutions for slope correction (pH 4 and 7) and temperature compensation. The accuracy for pH was estimated at ±0.05 (1 SD) based on periodic measurements of calibration standards. The mineralogy of the solid products was determined using a Rigaku Gigerflex X-ray diffractometer. Silicon was used as an internal standard for each analysis for correction of instrumental offset in 2θ value.

A small aliquot of the solid product from each experiment was mounted in epoxy, polished, and examined using a Cameca SX-50 electron microprobe for determination of crystal morphology and chemical composition of the Mg-calcite overgrowth. The Mg content of the overgrowth was determined based on backscatter electron (BSE) images, wavelength dispersive spectroscopy (WDS) elemental images, and standard electron microprobe (EMP) spot/point (2–3 μm) analysis. Analysis of areas smaller than the EMP spot size was accomplished using a refined defocused beam, by selecting WDS scanning data collected in raster mode at relatively high magnification for an area of interest that contained Mg. United States National Museum carbonate minerals were used as standards. Analytical uncertainty is about ±1% for major oxides (e.g., Mg and Ca).

2.2.2. Experimental procedure

Prior to each experiment, 500–1000 mL of mixed stock solution (referred to as master solution hereafter) was equilibrated with 100% CO_2 gas by bubbling the solution in a reaction vessel. This was done to ensure that the solution was undersaturated with respect to calcite, aragonite and dolomite and that no precipitation occurred before the experiment; after bubbling with 100% CO_2 gas, the pH of the master solutions ranged from 5.5 to 5.9. Thereafter the solutions were re-equilibrated with a CO_2/N_2 gas mixture by bubbling the solution at constant temperature (±0.02 °C) in a water bath until chemical equilibrium was achieved (i.e., pH remained constant for ~1 h). This was done to reset the chemical composition of the solution to attain a metastable state of supersaturation with respect to calcite at a pre-selected P_{CO_2} that precluded spontaneous nucleation of a solid phase. Once chemical equilibrium was attained, 80 mg of pure calcite seed crystals were added to the master solution to initiate heterogeneous surface-controlled growth of solid Mg-calcite at slightly supersaturated conditions. The seed crystals were Mg-free within detection limits of EMP analysis (<0.005 wt% Mg) and had a size range of 5–15 μm. The master solution was bubbled continuously with a specified CO_2/N_2 gas mixture (P_{CO_2} ranged from 0.038% to 3%) throughout the experiments (2–8 day). For experiments of longer duration (38–58 days), an airtight lid was secured to the reaction vessel, and bubbling was stopped after introduction of seed crystals. In these free-drift experiments, Mg-bearing calcite was precipitated from the master solution as overgrowths on the calcite seed crystals as the chemical composition of the solution drifted towards chemical equilibrium. Details of the experimental conditions are tabulated in Table 2.

A chemo-stat experiment was performed to evaluate the chemical characteristics of an overgrowth grown at true constant chemical composition throughout the duration of an experiment (for details, see Romanek et al., 1992). Synthesis of Mg-calcite took place in a vessel that contained 500 mL of master solution that was constantly stirred and bubbled using a CO_2/N_2 mixture with P_{CO_2} of 3%. Titrants (separate reservoirs of $MgCl_2$–$CaCl_2$ and $NaHCO_3$ solutions) were fed into the reaction vessel at a constant rate after addition of 80 mg of calcite seed crystals to maintain constant pH and compensate for the uptake of ions by Mg-calcite precipitation (Table 2). By such measures, the solution chemistry, precipitation rate, and precipitate mineralogy were kept constant throughout the experiment.

At the conclusion of an experiment the solids were separated from solution using a 0.45 μm filter, and a 23 mL aliquot of solution was acidified with 1 M HCl for later Mg isotope analysis. Solid products were cleaned from all components of the reaction vessel and filtration apparatus that were in contact with the solution, and the precipitate was washed briefly with de-ionized water and methanol on the filter before placing the filter in an oven to be dried at 40 °C overnight. Recovery of the solid was between 97% and 100% for control tests.

The aqueous chemistry and saturation state (with respect to pure calcite) of initial and final solution composition was modeled using Geochemist's Workbench. The observed equilibrium pH always matched the theoretical value based on solution chemistry (i.e., aqueous dissolved constituent concentrations determined by reagent mass and stoichiometry, solvent weight, P_{CO_2} of the gas phase bubbled through the solution and temperature). Final solution chemistry and saturation state were determined through analysis of aqueous Ca and Mg (by ICP-MS), total alkalinity (by titration), pH, and the P_{CO_2} of the gas phase bubbled through each master solution.

3. Results

3.1. Solution composition

In general, solution pH was higher for experiments buffered with lower P_{CO_2}, as expected. For the free-drift experiments, the

Table 2
Conditions of free drift and chemo-stat experiments.

Exp. no.	T (°C)	P_{CO_2} (%)	Δ^{26}Mg (‰)	Starting pH	Predicted equil. pH	Initial Ca conc. (mMol/L)	Initial Mg conc. (mMol/L)	Mg/Ca molar ratio	Initial alkalinity (N)	Exp. duration (h)	End-ing pH	Seed crystal (mg)	Overgrowth (mg)	Final Ca conc. (mMol/L)	Final Mg conc. (mMol/L)	Final alkalinity (N)	Mg content WDS (mol%)	1 SD	n	Mg content bulk disolu. (mol%)	Growth rate r (mmol/h/m^2)	log r	Satur. state of calcite before Exp.	Satur. state of calcite after Exp.
4c[b]	4	0.038	−2.70	5.59	8.40	2.65	29.74	11.2	0.002	912	8.32	82.0	16.6	2.46	29.72	0.002	0.8	0.4	28	1.5	4.4	0.64	2.4	2.2
10b	10	0.3	−2.73	5.71	7.82	15.48	47.93	3.1	0.010	192	7.89	87.8	83.8	13.88	47.78	0.006	5.4	0.7	22	4.6	98.2	1.99	15.9	8.9
15a	15	1.6	−2.68	5.62	7.54	14.86	49.69	3.3	0.010	168	7.56	85.3	51.2	13.73	49.59	0.008	9.1	2.3	34	8.1	71.0	1.85	9.4	7.4
C-22	22	3	−2.54	5.84	7.14	14.98	50.21	3.4	0.010	151	7.14	78.7	56.0	14.65	50.08	0.010	7.3	0.4	25	7.3	93.4	1.97	4.7	4.6
22a[a]	22	1.6	−2.54	5.55	7.35	14.55	50.50	3.5	0.010	168	7.32	79.0	224.8	10.73	50.33	0.004	8.8	0.7	16	7.6	302.9	2.53	7.4	2.2
22c	22	3	−2.62	5.85	7.34	15.34	48.70	3.2	0.010	72	7.37	81.0	27.7	14.76	48.68	0.009	1.9	0.5	16	2.2	93.3	1.97	7.7	7.2
22d[b]	22	3	−2.51	5.65	7.10	14.77	49.95	3.4	0.010	1296	6.75	82.4	40.5	14.42	49.88	0.007	7.1	1.5	33	6.1	7.5	0.88	4.2	2.9
22e[b]	22	3	−2.58	5.65	7.00	12.10	39.56	3.3	0.008	1296	6.81	86.0	4.0	12.07	39.55	0.007	1.4	0.5	20	0.9	0.7	−0.15	2.5	1.4
30a	30	1.6	−2.45	5.48	7.48	14.64	49.77	3.4	0.010	48	7.57	87.7	70.7	13.14	49.63	0.006	10.1	2.1	28	9.2	334.4	2.52	12.7	8.7
30b	30	3	−2.42	5.85	7.40	15.34	48.70	3.2	0.010	72	7.42	78.2	34.6	14.71	48.64	0.008	3.9	0.6	17	5.0	121.1	2.08	11.1	9.1
32a[b]	32	0.038	−2.45	5.59	8.65	3.89	50.25	12.9	0.004	1080	8.25	82.1	24.9	3.54	50.23	0.002	6.1	1.9	20	5.1	5.6	0.74	21.2	4.3
32b[b]	32	0.038	−2.32	5.59	8.60	3.27	39.52	12.1	0.003	1080	8.20	87.9	19.0	3.17	39.50	0.002	1.3	0.7	35	1.7	3.9	0.59	13.9	3.9
32d[b]	32	3	−2.49	5.65	7.10	14.77	49.95	3.4	0.010	1392	6.65	80.2	89.2	13.71	49.79	0.006	11.6	3.9	44	11.5	15.9	1.20	5.7	1.2
32f[b]	32	3	−2.35	5.65	6.90	9.06	30.06	3.3	0.006	1392	6.78	78.9	34.5	8.47	30.03	0.003	14.9	4.4	38	7.7	6.3	0.80	1.7	0.6
35a	35	1.6	−2.54	5.62	7.46	14.86	49.69	3.3	0.010	48	7.26	80.5	76.4	13.49	49.42	0.006	12.8	2.5	21	12.4	395.4	2.60	14.1	5.1
40a[a]	40	1.6	−2.42	5.56	7.42	15.58	47.38	3.0	0.010	48	7.24	85.8	120.9	13.39	47.20	0.006	4.8	1.2	29	4.0	521.6	2.76	15.6	5.6
40b	40	3	−2.46	5.90	7.42	14.92	50.29	3.4	0.010	30	7.40	80.0	70.1	13.53	50.16	0.008	8.6	0.7	13	7.1	580.1	2.76	14.7	10.4
40c[a]	40	3	−2.47	5.85	7.47	15.34	48.70	3.2	0.010	72	7.27	81.7	120.0	12.88	51.07	0.007	6.1	0.7	16	5.1	363.2	2.61	17.1	6.5
45a[a]	45	1.6	−2.23	5.48	7.59	14.64	49.77	3.4	0.010	48	7.33	88.9	152.9	11.90	49.63	0.005	4.4	1.0	27	3.3	636.2	2.85	24.3	5.8
45b	45	3	−2.22	5.78	7.03	15.41	49.65	3.2	0.007	52	6.97	81.3	21.3	15.19	49.60	0.006	2.8	1.2	24	3.0	99.2	2.00	5.1	3.8
45c	45	3	−2.24	5.95	7.26	9.65	39.41	4.1	0.010	52	7.07	86.6	80.1	8.53	39.23	0.006	7.2	0.8	26	4.5	352.5	2.55	8.7	3.1

C-22: Chemo-stat experiment, others are free-drift experiments.
N/A: not analyzed.

[a] Experiments have less than 10% aragonite in solid phase, growth rates were calculated using a subtraction of 10% of total overgrowth amount.
[b] Long term experiment, not bubbled continuously throughout the experiment.

pH of the solutions decreased over time due to precipitation of Mg-calcite (Table 2). The final pH of each synthesis experiment was close to the theoretical estimate, indicating the solution chemistry was accurately characterized. The change in aqueous Mg concentration over the course of each experiment was insignificant ($<0.5\%$), because the reservoir of aqueous Mg was large compared to the proportion precipitated in the solid phase. In terms of Mg, therefore, the free-drift experiments were essentially precipitating from an infinite reservoir. In contrast, Ca concentrations decreased by up to 26% during the experiments (Table 2), due to precipitation of carbonate, accompanied by a decrease in total alkalinity in a 1:2 ratio to maintain charge balance. The chemical composition of the fluid in the chemo-stat experiment remained constant throughout the experiment (Table 2), reflecting steady-state conditions.

3.2. Synthesis products

The mass of Mg-calcite produced in the experiments was calculated by subtracting the weight of seed crystals from the weight of recovered solid products (Table 2). SEM and XRD analyses confirmed that calcite and Mg-calcite were the only minerals in the solid products for the chemo-stat experiment and most of the free-drift experiments. In four experiments, minor aragonite was identified in the solid products (Table 2). Grains of the final solid were typically between 5 μm and 15 μm in diameter and had euhedral to subhedral shapes (Fig. 2). Unlike the seed material, surfaces of the solid products were rough and displayed numerous steps and domains. Incorporation of Mg in newly precipitated calcite was verified by a shift in the (104) d-spacing for calcite in XRD patterns. BSE and WDS mapping of Mg in polished sections of the solid products indicated the formation of Mg-calcite overgrowth on the pure calcite seed crystals (Fig. 2). The thickness of Mg-bearing calcite overgrowth varied from 0.1 μm to 2 μm. The mole percentage of $MgCO_3$ in the overgrowth was determined by bulk dissolution, EMP spot analysis and defocused beam analysis, and the values ranged from 0.8 to 14.9 mol% (Table 2). No correlation was found between the Mg content and/or weight of the overgrowths with pH, reaction time, and composition of solution (Table 2).

Table 2 reports average precipitation rate in $\mu mol\,m^{-2}\,h^{-1}$ based on the mass of overgrowth, the mole percentage of $MgCO_3$ (as determined by WDS analysis in the overgrowth), the surface area of the seed crystals ($0.5\,m^2\,g^{-1}$; Romanek et al., 1992), and the duration of the experiment. It is important to note that the instantaneous precipitation rate during an experiment likely varied from the average rate for all the free drift experiments. For example, the average precipitation rate likely underestimates the instantaneous rate early in the experiment, whereas it is overestimated close to the termination of an experiment. If there was an initial rapid precipitation that produced a kinetic isotope fractionation, this could mask possible equilibrium isotope fractionation later in the experiment, depending on the mass of solid produced during different stages of growth. Therefore, the average precipitation rate provides only broad constraints on possible kinetic effects on isotope fractionation. In contrast, the chemo-stat experiment is not hampered by such problems because the overall conditions of the experiment do not change over the duration of the experiment.

Variations in Mg WDS intensity mapping of polished carbonate samples from free-drift experiments indicate compositional heterogeneity in the Mg-bearing calcite overgrowth (Fig. 2). For samples that have >10 mol% Mg overgrowth, multiple EMP spot analyses and defocused beam analyses revealed a 2.1–4.4 mol% standard deviation, whereas samples that have <10 mol% Mg overgrowth (Table 2) have 0.4–3.5 mol% standard deviation. Compositional variability of Mg-bearing overgrowths in free-drift experiments has been reported previously, and has been attributed to changes in solution composition over time (Jimenez-Lopez et al., 2004).

3.3. Magnesium isotope composition of reactants and products

A single Mg stock solution was used for all experiments and the average $\delta^{26}Mg$ value of 11 replicate samples was -1.73 ± 0.08‰ (2 SD; Table 3). The Mg isotope composition of the solution at the end of

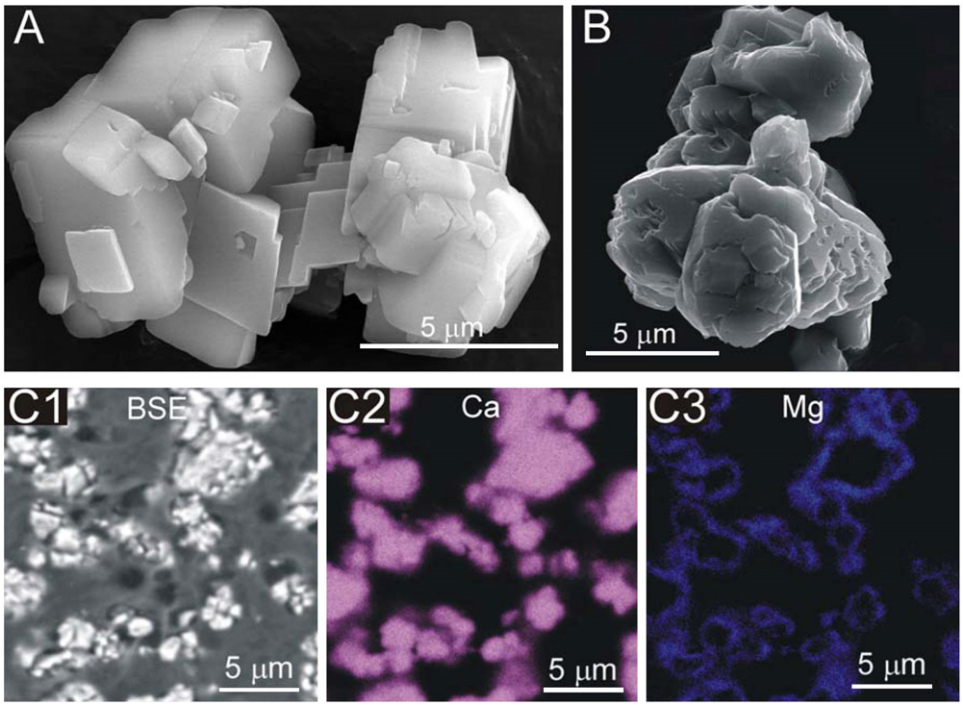

Fig. 2. (A) Secondary electron image (SEM) of Mg-free calcite seed crystals displaying rhombic habit. (B) Representative SEM image of final solid products with Mg-calcite overgrowth (from Exp. 30a). C1, C2, and C3 are representative backscatter electron image and wavelength dispersive spectroscopy (WDS) scan maps of Ca and Mg for the final solid products (from Exp. 30a), respectively. Mg WDS map clearly shows no Mg in the core of the crystals.

Table 3
Magnesium isotope composition of solutions and carbonates in synthesis experiments and corresponding isotope fractionation factors.

Exp no.	P_{CO_2} (%)	Mg/Ca	T (°C)	Solution								Carbonates								Fractionation					
				$\delta^{26/24}$Mg	2 SD	$\delta^{25/24}$Mg	2 SD	$\delta^{26/25}$Mg	2 SD	n	N	$\delta^{26/24}$Mg	2 SD	$\delta^{25/24}$Mg	2 SD	$\delta^{26/25}$Mg	2 SD	n	N	$\Delta^{26/24}$Mg	2 SD	$\Delta^{25/24}$Mg	2 SD	$\Delta^{26/25}$Mg	2 SD
Initial solution																									
				−1.73	0.08	−0.89	0.05	−0.84	0.04	39	11														
Final solution																									
4c	0.038	11.2	4	−1.78	0.01	−0.84	0.11	−0.92	0.09	2	1	−4.48	0.24	−2.29	0.14	−2.19	0.09	3	1	−2.70	0.24	−1.45	0.18	−1.27	0.13
10b	0.3	3.1	10	−1.72	0.15	−0.88	0.13	−0.82	0.02	3	1	−4.45	0.05	−2.32	0.26	−2.17	0.10	6	2	−2.73	0.16	−1.44	0.29	−1.35	0.10
15a	1.6	3.3	15	−1.71	0.17	−0.88	0.12	−0.84	0.08	5	2	−4.39	0.06	−2.25	0.05	−2.14	0.06	6	1	−2.68	0.18	−1.41	0.13	−1.30	0.10
C-22	3.0	3.4	22	−1.68	0.22	−0.87	0.12	−0.82	0.10	7	2	−4.23	0.15	−2.17	0.09	−2.06	0.10	10	2	−2.54	0.27	−1.30	0.15	−1.24	0.14
22a	1.6	3.5	22	−1.69	0.02	−0.91	0.06	−0.78	0.05	2	1	−4.23	0.09	−2.19	0.05	−2.04	0.07	17	4	−2.54	0.09	−1.28	0.08	−1.26	0.09
22c	3.0	3.2	22	−1.79	0.16	−0.92	0.09	−0.87	0.07	3	1	−4.42	0.08	−2.28	0.11	−2.15	0.09	7	2	−2.62	0.18	−1.36	0.14	−1.28	0.12
22d	3.0	3.4	22	−1.75	0.16	−0.89	0.13	−0.84	0.01	2	1	−4.25	0.16	−2.18	0.12	−2.06	0.09	3	1	−2.51	0.22	−1.29	0.17	−1.22	0.09
22e	3.0	3.3	22	−1.73	0.08	−0.89	0.05	−0.84	0.04	**		−4.33	0.13	−2.23	0.10	−2.11	0.10	1*	1	−2.59	0.15	−1.34	0.11	−1.28	0.11
30a	1.6	3.4	30	−1.83	0.16	−0.94	0.11	−0.89	0.05	6	2	−4.28	0.06	−2.19	0.07	−2.08	0.04	4	1	−2.45	0.17	−1.26	0.13	−1.19	0.06
30b	3.0	3.2	30	−1.73	0.09	−0.88	0.06	−0.85	0.06	7	2	−4.14	0.20	−2.15	0.13	−2.00	0.12	13	3	−2.42	0.22	−1.27	0.14	−1.15	0.13
32a	0.038	12.9	32	−1.73	0.08	−0.89	0.05	−0.84	0.04	**		−4.20	0.17	−2.17	0.06	−2.06	0.12	3	1	−2.47	0.18	−1.27	0.08	−1.22	0.13
32b	0.038	12.1	32	−1.82	0.16	−0.96	0.22	−0.83	0.09	2	1	−4.15	0.08	−2.16	0.04	−2.02	0.04	2	1	−2.32	0.18	−1.20	0.22	−1.19	0.10
32d	3.0	3.4	32	−1.74	0.03	−0.87	0.04	−0.84	0.01	2	1	−4.23	0.18	−2.17	0.05	−2.06	0.16	3	1	−2.49	0.18	−1.29	0.07	−1.22	0.16
32f	3.0	3.3	32	−1.77	0.10	−0.90	0.03	−0.88	0.08	2	1	−4.13	0.08	−2.14	0.07	−2.00	0.05	3	1	−2.35	0.13	−1.24	0.08	−1.13	0.10
35a	1.6	3.3	35	−1.67	0.19	−0.87	0.07	−0.80	0.13	6	2	−4.22	0.16	−2.16	0.08	−2.06	0.07	12	4	−2.54	0.25	−1.30	0.10	−1.25	0.15
40a	1.6	3.0	40	−1.68	0.06	−0.86	0.07	−0.82	0.06	4	1	−4.10	0.16	−2.10	0.12	−1.99	0.07	10	2	−2.42	0.17	−1.24	0.14	−1.17	0.09
40b	3.0	3.4	40	−1.73	0.15	−0.89	0.08	−0.84	0.10	16	4	−4.20	0.24	−2.17	0.15	−2.03	0.13	20	4	−2.46	0.28	−1.28	0.17	−1.19	0.16
40c	3.0	3.2	40	−1.72	0.10	−0.88	0.03	−0.83	0.08	14	3	−4.18	0.21	−2.16	0.14	−2.03	0.10	20	5	−2.47	0.23	−1.29	0.14	−1.20	0.12
45a	1.6	3.4	45	−1.81	0.14	−0.94	0.06	−0.90	0.06	2	1	−4.04	0.09	−2.08	0.05	−1.98	0.08	11	2	−2.23	0.16	−1.14	0.08	−1.08	0.10
45b	3.0	3.2	45	−1.80	0.18	−0.91	0.09	−0.90	0.13	3	1	−4.02	0.16	−2.10	0.07	−1.93	0.09	5	1	−2.22	0.24	−1.18	0.11	−1.02	0.16
45c	3.0	4.1	45	−1.77	0.20	−0.91	0.15	−0.88	0.07	6	1	−4.02	0.28	−2.08	0.12	−1.96	0.20	4	1	−2.24	0.34	−1.17	0.19	−1.07	0.21

N/A: not analyzed.
n: number of analyses.
N: number of replicates.

* Only one measurement was carried out, used long tern external reproducibility of Mg isotope analysis for analytical error.
** Did not analyze solution, used the average Mg isotope composition of starting solution.

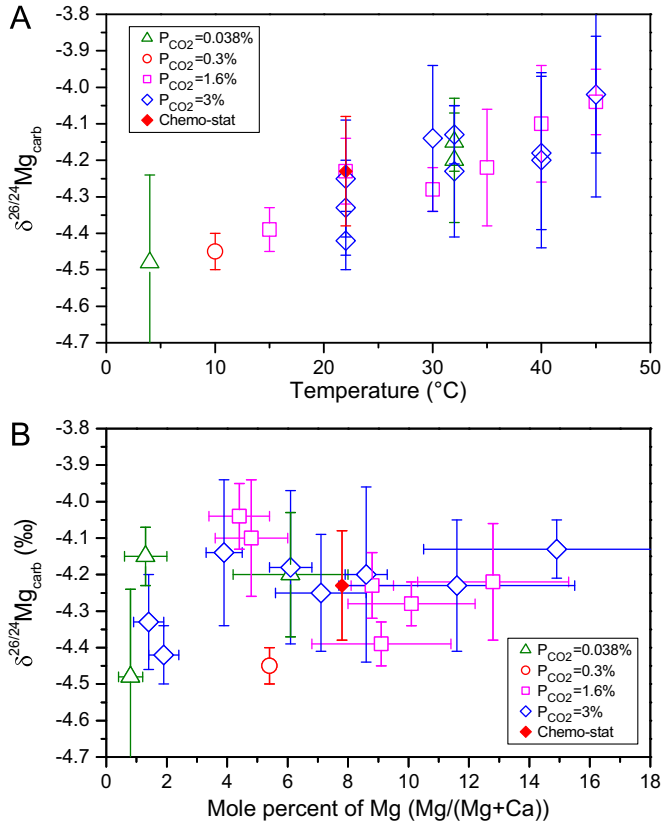

Fig. 3. Variation of Mg isotope composition of Mg-bearing calcite overgrowth versus temperature (A) and Mg content in carbonate (B).

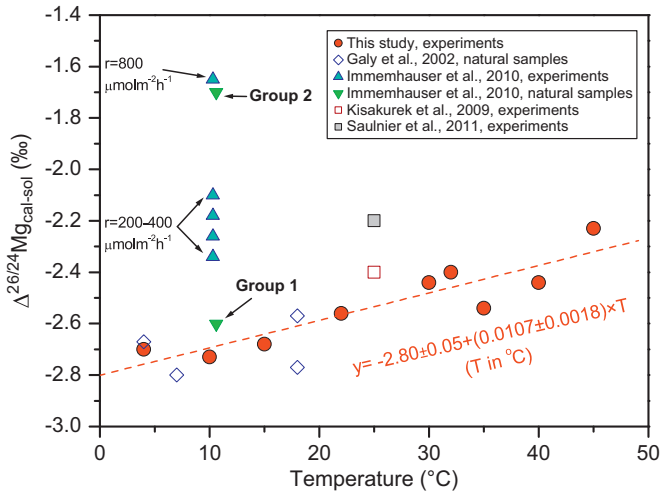

Fig. 4. Comparison of experimental determined $\Delta^{26}Mg_{cal-sol}$ values (where multiple experiments were done at the same temperature, an average value is plotted) with fractionation factors reported by other experimental and field studies. Errors of these data are typically within 0.1–0.2‰. The precipitation rates (r) for synthesized Mg-bearing calcite reported by Immenhauser et al. (2010) are noted. Immenhauser et al. (2010) reported three groups of samples from natural environments, among which, Group 1 are slowly precipitated speleothem samples, and Group 2 are surficial calcrete (calcareous crust) of a speleothem that are suggested to be precipitated at higher rates; Group 3 data are omitted because of potential contamination concerns (A. Immenhauser, personal communication, 2012).

each experiment was measured and its isotope composition ($\delta^{26}Mg = -1.75 \pm 0.09$‰; 2 SD, $N=19$; Table 3) was identical to that of the starting solution, reflecting the fact that during precipitation of Mg-bearing calcite >99% of the Mg budget is retained in the solution. In contrast, the precipitated carbonates have $\delta^{26}Mg$ values that range from −4.02‰ for Exp. 45b to −4.48‰ for Exp. 4c (Table 3). Multiple experiments were run at temperatures of 22 °C, 30 °C, 32 °C, 40 °C and 45 °C, and, in general, Mg-bearing carbonates synthesized at the same temperature have similar Mg isotope compositions (Table 3, Fig. 3a), despite differences in P_{CO_2} and Mg concentration in the initial solution, as well as the mole percentage of Mg in the overgrowth (Fig. 3b; Table 2). Overall, temperature appears to have the strongest control on Mg isotope composition of the overgrowth, and there is a positive correlation between the $\delta^{26}Mg$ measured in carbonate and temperature (Fig. 3a), although this control is mild, as discussed below.

4. Discussion

4.1. Temperature dependence of Mg isotope fractionation between calcite and aqueous solution

The Mg isotope fractionation factor between calcite and aqueous Mg was calculated using the difference in isotopic composition between calcite and the final isotopic composition of aqueous Mg, defined as $\Delta^{26/24}Mg_{cal-sol}$ (Eq. (2); Table 3). There is a negative correlation between $\Delta^{26/24}Mg_{cal-sol}$ and $10^6/T^2$ (Appendix 2), and the best fit to these data as calculated using *IsoPlot* (Ludwig, 1999) is

$$\Delta^{26/24}Mg_{cal-sol} = (-0.158 \pm 0.051) \times 10^6/T^2 - (0.74 \pm 0.56)$$

with a mean square weighted deviation (MSWD) of 0.95, where T is in Kelvin. The Mg isotope fractionation factor between calcite and aqueous Mg therefore has a small, but significant temperature dependency, where the fractionation factor varies by 0.011‰/°C in $^{26}Mg/^{24}Mg$ over the temperature range 4–45 °C (Fig. 4). This is consistent with Galy et al. (2002) who reported the fractionation factor as a function of mean annual cave temperature. Importantly, our $\Delta^{26/24}Mg_{cal-sol}$ fractionations at a given temperature do not show a correlation with Mg content in the overgrowth or P_{CO_2}, suggesting that the fractionation factor is relatively insensitive to compositional variations, at least over the range of values explored in the current study.

It is important to note that the temperature dependence measured for the $\Delta^{26/24}Mg_{cal-sol}$ fractionations matches that expected for an equilibrium relation, where the fractionation increases with decreasing temperature (e.g., Schauble, 2004). If the temperature dependency of the current experiments is extrapolated to infinite temperature, the intercept is -0.76 ± 0.51 (Appendix 2). Despite the very large temperature extrapolation, the intercept is close to the expected zero fractionation at infinite temperature, a relation that is consistent with theory for equilibrium isotope fractionation (e.g., Schauble, 2004).

4.2. Kinetic effects

The kinetic isotope effects observed during carbonate precipitation for various stable isotope systems reflect isotopic fractionations produced by rate-limiting steps. Kinetic isotope effects have been recognized to be associated with precipitation rate for O (e.g., de Villiers et al., 1995) and C isotopes (e.g., McConnaughey, 1989a) in carbonates. In the case of C, the rate-limiting step is isotopic exchange between gaseous and dissolved C, and for O, isotopic exchange between dissolved carbonate and water (Kim et al., 2006; McConnaughey, 1989b). The kinetic fractionation inferred for Ca isotopes (e.g., Lemarchand et al., 2004) likely reflects transport processes to the crystal surface. Unlike C and O isotopes, Ca and Mg isotope fractionation is expected to be relatively insensitive to the dissolved inorganic carbon (DIC) content because CO_2 is not a repository for Ca and Mg, and ion pairing (complexation) between

DIC and Ca^{2+} and Mg^{2+} is negligible in aqueous solution under most ambient conditions compared to free aqueous metal contents.

In this study, carbonate synthesis experiments at 32 °C were carried out under conditions where P_{CO_2} varied by nearly two orders of magnitude (0.038% for Exp. 32a–c to 3% for Exp. 32d–f; Table 2), the Mg content of solutions varied nearly two-fold (~30 mM L^{-1} for Exp. 32c to ~50 mML^{-1} for Exp. 32a), and the Mg/Ca molar ratio varied four-fold (3.0 for Exp. 32f to 12.1 for Exp. 32b). On the other hand, the fractionation factors measured for these experiments are similar (Table 3). This confirms the expectation that Mg isotope fractionation is unrelated to carbon dioxide–carbonate ion exchange. This is consistent with the observations of Saulnier et al. (2011), who reported that the $\Delta^{26}Mg_{carb\text{-}sol}$ fractionation of -2.2 ± 0.2‰ is independent of pH and Mg/Ca ratio of solutions in their experiments.

Kinetic Mg isotope fractionation due to solution transport to the crystal interface, as well as dehydration from solution, may explain the sensitivity of Mg isotope fractionation to precipitation rate observed by Immenhauser et al. (2010), who reported $\Delta^{26/24}Mg_{cal\text{-}sol}$ fractionations at 10 °C that varied from −2.33 to −1.63‰ as a function of precipitation rate (200–800 μmol m^{-2} h^{-1}; Fig. 4). Moreover, large variations in the fractionation factor have been deduced from speleothem studies by Immenhauser et al. (2010), who report less negative $\Delta^{26/24}Mg_{cal\text{-}sol}$ fractionations for speleothem formed at more rapid precipitation rates. Analysis of bulk speleothems and cave water in which precipitation rates were inferred to have been relatively slow (Galy et al., 2002; Immenhauser et al., 2010) produced $\Delta^{26/24}Mg_{cal\text{-}sol}$ fractionations that are similar to those determined in our synthesis experiments (Fig. 4).

The precipitation rate for the chemo-stat experiment at 22 °C is well constrained at 93 μmol $m^{-2}h^{-1}$. This is significantly lower than the rates reported by Immenhauser et al. (2010), which may explain their generally less negative $\Delta^{26/24}Mg_{cal\text{-}sol}$ fractionations. As noted above, precipitation rates for the free-drift experiments are difficult to constrain for comparison, but the average precipitation rates at 22 °C ranged from <1 to 303 μmol $m^{-2}h^{-1}$ (Table 2). Despite the uncertainty in rate, all of these experiments produced identical $\Delta^{26/24}Mg_{cal\text{-}sol}$ fractionations. It is noteworthy that Kisakurek et al. (2009) reported that the $\Delta^{26/24}Mg_{cal\text{-}sol}$ fractionation did not vary over precipitation rates ranging from 100 to 10,000 μmol $m^{-2}h^{-1}$. We conclude that although kinetic effects are potentially important, it is unlikely to be the major source of variability in Mg isotope fractionation during calcite precipitation for our experiments.

The combination of: (1) relatively low precipitation rate of the chemo-stat experiment, (2) the use of seed crystals to lower the activation energy for heterogeneous nucleation, and (3) the attendant decrease in the degree of supersaturation required to promote calcite precipitation (Mullin, 2001), suggests that our experimental data may estimate equilibrium Mg isotope fractionation for the Mg-calcite system. Because carbonate precipitation is a unidirectional process, it is not possible to rigorously prove that isotopic equilibrium was attained. As an analog, Ca isotope fractionation between calcite and aqueous Ca has been debated for years, and very different Ca isotope fractionation factors have been proposed from experimental (e.g., Lemarchand et al., 2004) and field (e.g., Fantle and DePaolo, 2007) studies. Nevertheless, we note that the Mg isotope fractionation factors between calcite and aqueous Mg determined in this study are consistent with those deduced by analysis of solid carbonate and cave water for slow growing speleothems (Galy et al., 2002; Immenhauser et al., 2010; Fig. 4), and the consistency of our results over wide ranges in experimental conditions suggests that the results may approximate equilibrium conditions.

4.3. Comparison with calculated fractionation factors

In contrast to the agreement between $\Delta^{26/24}Mg_{cal\text{-}sol}$ fractionations determined from our experiments and those deduced from analysis of bulk speleothems and cave water, the Mg isotope fractionation factors between calcite and aqueous Mg calculated by *ab initio* methods are distinct (Fig. 5a). The calculated $\Delta^{26/24}Mg_{cal\text{-}sol}$ fractionations using the β values from Rustad et al. (2010) for calcite and aqueous Mg are greater in magnitude (more negative) than those measured in the current study. An even more negative $\Delta^{26/24}Mg_{cal\text{-}sol}$ fractionation is calculated when the β value for aqueous Mg from Schauble (2011) and the β value for calcite from Rustad et al. (2010) are combined (Fig. 5a). The fractionation factors calculated for other Mg-bearing carbonates, including magnesite and dolomite, all have higher $\Delta^{26/24}Mg_{carbonate\text{-}sol}$ fractionations, where both Rustad et al. (2010) and Schauble (2011) predict that $\Delta^{26/24}Mg_{dolomite\text{-}sol} > \Delta^{26/24}Mg_{magnesite\text{-}sol}$. There is, however, little agreement between carbonate-solution fractionation factors for specific minerals. For example, Rustad et al. (2010) predicts that $\Delta^{26/24}Mg_{dolomite\text{-}sol} > 0$, whereas Schauble (2011) predicts $\Delta^{26/24}Mg_{dolomite\text{-}sol} < 0$ (Fig. 5a). Based on Mg isotope compositions of deep-sea sediment pore-fluids and dolomite from ODP drill cores 1082 and 1012, Higgins and Schrag (2010) suggested that $\Delta^{26/24}Mg_{dolomite\text{-}sol}$ varies between −2.0‰ and −2.7‰, which is closer to the modeling results of Schauble

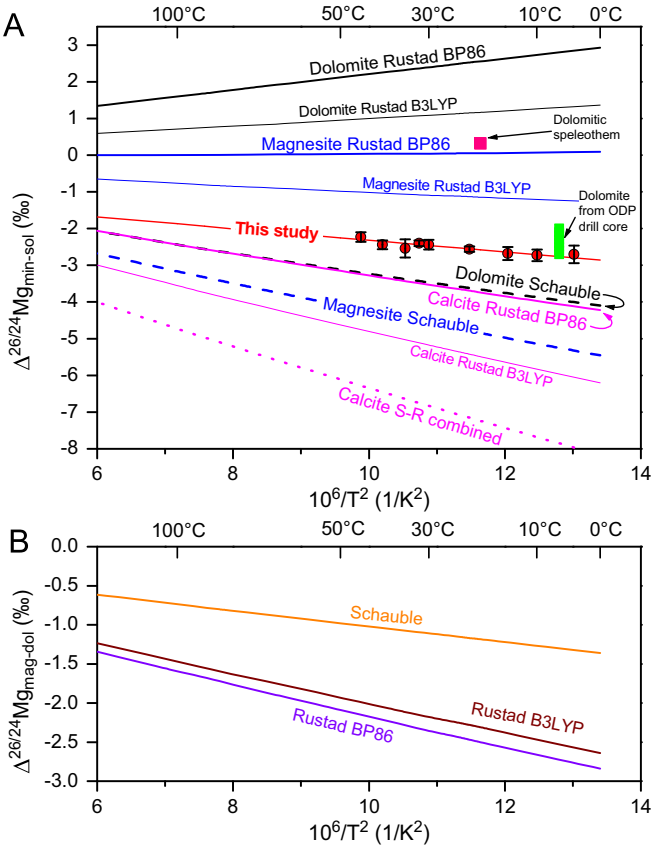

Fig. 5. (A) Comparison of theoretically predicted Mg isotope fractionation factors between carbonates and solution ($\Delta^{26/24}Mg_{min\text{-}sol}$) with data determined from this experiments and previous field studies. The fractionation factors for calcite, dolomite, and magnesite were calculated by Rustad et al. (2010) using two different models (BP86 and B3LYP). Schauble (2011) also calculated $\Delta^{26/24}Mg_{min\text{-}sol}$ for dolomite and magnesite. In addition, the β factor for calcite calculated by Rustad et al. (2010) using BP86 model is combined with the β factor for aqueous Mg by Schauble (2011) to generate a third prediction of $\Delta^{26/24}Mg_{min\text{-}sol}$ for calcite (denoted as "Calcite S-R combined"). The apparent $\Delta^{26/24}Mg_{min\text{-}sol}$ for dolomite from ODP drill cores are from Higgins and Shrag (2010), temperature is arbitrarily assumed at 6 °C. The apparent $\Delta^{26/24}Mg_{min\text{-}sol}$ for dolomitecalcite speleothem sample was reported by Galy et al. (2002). (B) Comparison of theoretically predicted Mg isotope fractionation factors between magnesite and dolomite ($\Delta^{26/24}Mg_{mag\text{-}dol}$) calculated by Schauble (2011) and Rustad et al. (2010), the latter used two different models (BP86 and B3LYP) in their calculation.

(2011) than those of Rustad et al. (2010). The fractionation factor inferred by Galy et al. (2002) from a speleothem that was composed of a mixture of calcite and dolomite and cave water yields a $\Delta^{26/24}Mg_{carbonate\text{-}sol}$ of +0.33‰, which seems to agree better with the dolomite-fluid fractionation factors calculated by Rustad et al. (2010).

A possible explanation for the disparity between experimentally determined and calculated $\Delta^{26/24}Mg_{cal\text{-}sol}$ fractionations is differences in Mg bonding as a function of composition; such an effect is expressed for O and C isotopes, where $\Delta^{18}O_{cal\text{-}sol}$ and $\Delta^{13}C_{cal\text{-}sol}$ fractionations correlate with Mg content in calcite (Jimenez-Lopez et al., 2006, 2004). In the Rustad et al. (2010) calculations for Mg isotope fractionation in calcite, Mg was modeled as an infinitely dilute Mg^{2+} solid solution in calcite, therefore a pure calcite lattice configuration was used. In contrast, substitution of Ca^{2+} with Mg^{2+} has a significant impact on the calcite lattice (e.g., Bischoff et al., 1983; Zhang et al., 2010), and indeed the shift in the (104) d-spacing is roughly proportional to the amount of Mg in the calcite structure. Such d-spacing changes should produce changes in relative bond strengths and angles, and hence could impact calculated isotope fractionation factors (O'Neil, 1986). Contrary to this line of argument, however, is the observation in our experimental results that at a given temperature there are no significant changes in $\Delta^{26/24}Mg_{cal\text{-}sol}$ fractionations from 0.8 to 14.9 mol% Mg in calcite, so it is unclear what effect calcite lattice changes caused by Mg substitution have on Mg isotope fractionation factors.

There is closer agreement among calculated Mg isotope fractionation factors between two minerals as compared to mineral-fluid fractionation factors. The $\Delta^{26/24}Mg_{magnesite\text{-}dolomite}$ fractionation calculated by Rustad et al. (2010) using two different models agree closely with each other, and they are within 1.2‰ of the $\Delta^{26/24}Mg_{magnesite\text{-}dolomite}$ fractionation calculated by Schauble (2011) (Fig. 5b). This contrast between experimental and calculated fractionation factors has also been observed for Fe isotopes. Calculated fractionation factors of mineral-fluid systems are difficult to evaluate due to the effects of multiple hydration spheres around an aqueous metal species (e.g., Rustad et al., 2010; Beard et al., 2010). We speculate that these effects are part of the reason for differences in the calculated fractionation factors between dolomite, magnesite, and aqueous Mg as compared to the dolomite–magnesite system. Such effects may be compounded by crystal lattice changes that may influence isotopic fractionation. We conclude that further work is clearly needed to reconcile experimentally determined and calculated Mg isotope fractionation factors for carbonates. Such reconciliation is important, because calculated fractionation factors, if pinned at specific experimental conditions, allow extrapolation to conditions that may be unapproachable by experiments.

4.4. Comparison to biologically-catalyzed carbonate precipitation

This study experimentally assessed the influence of temperature, solution composition, P_{CO_2}, and precipitation rate on $\Delta^{26/24}Mg_{cal\text{-}sol}$ fractionations, and therefore provides a baseline for inorganic carbonate formation that may be used to compare with Mg isotope studies on biologically catalyzed carbonate precipitation. For marine calcifiers, the $\Delta^{26/24}Mg_{carbonate\text{-}sol}$ fractionations vary from −5.34 to −0.24‰ (Chang et al., 2004; Hippler et al., 2009; Müller et al., 2011; Pogge von Strandmann, 2008; Ra et al., 2010; Wombacher et al., 2006, 2011; Fig. 6). Although some of the Mg isotope variability may be a function of the temperature (Hippler et al., 2009; Fig. 6), most of the variability is attributed to species differences and mineralogy (Chang et al., 2004; Wombacher et al., 2006; Pogge von Strandmann, 2008; Hippler et al., 2009; Ra et al., 2010; Müller et al., 2011; Wombacher et al., 2011; Fig. 6). In general, the most negative $\Delta^{26/24}Mg_{cal\text{-}sol}$ fractionations are reported from low-Mg calcite, and the least negative $\Delta^{26/24}Mg_{cal\text{-}sol}$ fractionations are reported from aragonite, although there is some concern that Mg is not in the aragonite lattice (A. Immenhauser, personal communication, 2012). Moreover, high-Mg calcite tends to have intermediate fractionations (Wombacher et al., 2006, 2011; Hippler et al., 2009; Fig. 6), raising the possibility of formation via distinct pathways. In addition, there are significant variations in Mg isotope composition that are species dependent, where the most negative $\Delta^{26/24}Mg_{cal\text{-}sol}$ fractionations are associated with planktonic foraminifera, and the $\Delta^{26/24}Mg_{cal\text{-}sol}$ fractionations become more positive in the order of bivalves < red algae < echinoids < brachiopods. In addition, the $\Delta^{26/24}Mg_{carbonate\text{-}sol}$ fractionation for benthic foraminifera, coral, sponges, and coccolith ooze vary by several per mil, but they all have more positive $\Delta^{26/24}Mg_{carbonate\text{-}sol}$ values than planktonic foraminifera.

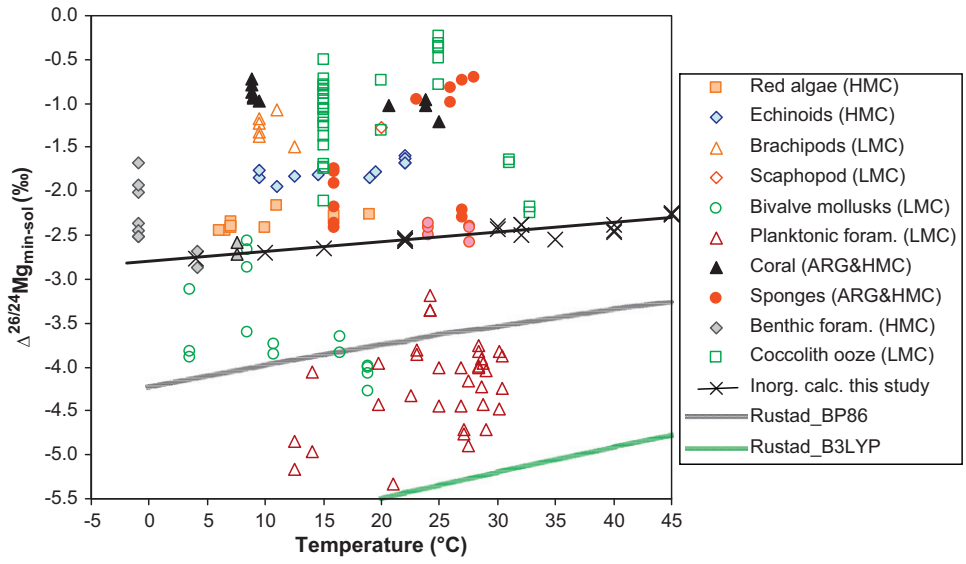

Fig. 6. Compilation of Mg isotope fractionation observed from marine organisms with known habitat temperature. Solid symbols note aragonite (ARG), open symbols note low magnesium calcite (LMC), symbols filled with light colors note high magnesium calcite (HMC). For comparison, experimentally determined (this study) and theoretically predicted Mg isotope fractionation factors are also plotted.

Existing data highlight so-called "vital" (biological) effects on Mg isotope fractionation during growth of marine calcifiers. The experimentally and theoretically determined $\Delta^{26/24}Mg_{carbonate\text{-}sol}-T$ trends for Mg-bearing inorganic calcite provide an important framework for further study. Certain species of benthic foraminifera (*Triloculina* sp., *milliloid* sp.; Wombacher et al., 2011), calcitic coral (*Keratoisis* sp.; Wombacher et al. 2011), and sponges (*Acanthochaetetes wellsi*; Wombacher et al., 2011) lie on the experimentally determined $\Delta^{26/24}Mg_{carbonate\text{-}sol}-T$ trend for inorganic carbonate in Fig. 6, which may imply that little or no "vital" effect is involved during skeletal growth. The majority of marine species plot above the inorganic carbonate trend, and, notably, data points for red algae and echinoids follow two trends that are parallel to the inorganic calcite trend, but offset by ca. 0.3‰ and 0.8‰, respectively. These observations suggest that distinct "vital" effects may characterize Mg isotope fractionations between species. Many mechanisms may account for the observed fractionations, such as kinetic isotope effects (Immenhauser et al., 2010) that are biologically promoted during skeleton growth, isotope fractionation during transport of Mg through the cell membrane (Black et al., 2008; Hippler et al., 2009), Mg isotope fractionation caused by bonding with bio-molecules within cells (Black et al., 2006, 2007; Bolou-Bi et al., 2010), and involvement of amorphous calcium carbonate as a transient precursor phase during skeleton growth (e.g., Wombacher et al., 2011, and reference therein). It is important to note that to date, only two faunal groups (planktonic foraminifera and bivalve mollusks) produce Mg isotope fractionations that are more negative than inorganic calcite. This is significant because this may imply that these two groups utilize a distinct mechanism for skeletal growth, which shifts Mg isotope fractionation in an opposite direction as compared with most other marine organisms.

5. Summary and conclusion

The Mg isotope fractionation between Mg-bearing calcite and Mg in aqueous solution has been measured over a range of temperatures using Mg-free seed calcite crystals to minimize kinetic effects that may be induced by spontaneous nucleation and highly supersaturated solutions. Synthesis of Mg-bearing calcite was conducted using a series of free-drift experiments and one chemo-stat experiment, the later providing a constant fluid composition during precipitation. The Mg isotope fractionations between Mg-bearing calcite and solution ($\Delta^{26/24}Mg_{cal\text{-}sol}$) correlate positively with temperature, varying from -2.70‰ at 4 °C to -2.22‰ at 45 °C and this defines a function of $\Delta^{26/24}Mg_{cal\text{-}sol}=(-0.158\pm0.051)\times10^6/T^2-(0.74\pm0.56)$, where T is temperature in Kelvin. Magnesium isotope fractionation factors do not correlate with Mg content in the carbonate overgrowth, suggesting that over the range of Mg contents studied (0.8–14.9 mol% Mg in calcite), the Mg isotope fractionation is constant. In addition, the measured Mg isotope compositions were independent of changes in P_{CO_2} and therefore invariant with respect to dissolved carbonate. The small temperature effect on $\Delta^{26/24}Mg_{cal\text{-}sol}$ fractionation and the insensitivity of $\Delta^{26/24}Mg_{cal\text{-}sol}$ to P_{CO_2}, solution chemistry, and calcite composition greatly simplifies the use of Mg isotopes in modern or ancient marine systems to constrain Mg fluxes, including continental weathering.

Because Mg isotope fractionation appears to be independent of P_{CO_2} and Mg concentration in carbonate, we believe these experiments may approximate an equilibrium Mg isotope fractionation between Mg-bearing calcite and aqueous Mg. Importantly, we note that the fractionation factor for the free drift experiments is similar to the results of a chemo-stat experiment conducted under similar conditions. Moreover, the fractionation factors measured in this study at an individual temperature closely match those of previous synthesis experiments and those deduced from natural samples in cave environments where fluid and carbonate compositions were measured. There is, however, >1‰ difference between the experimental and theoretically determined Mg isotope fractionation factors. This might indicate unresolved kinetic isotope fractionation in our experiments. Alternatively, the calculated reduced partition function ratios for calcite may need refinement by including a larger number of Mg atom substitutions, or better modeling of Mg^{2+} in solution.

Although there is a statistically significant correlation of the Mg isotope fractionation factor with temperature (0.011‰/°C) from 4 °C to 45 °C, the temperature effect is small and so application of Mg isotopes as a geothermometer may be difficult. In particular, this temperature effect is dwarfed by the range in Mg isotope fractionations produced by biologically-catalyzed carbonate formation in marine organisms, where $\Delta^{26/24}Mg_{cal\text{-}sol}$ fractionations of -5.34‰ to -0.24‰ have been observed from a variety of species living at a temperature range of -1 °C to 33 °C. Nevertheless, the trend of $\Delta^{26/24}Mg_{cal\text{-}sol}$ versus temperature as experimentally determined in this study serves as a fundamental baseline for assessing and interpreting effects of Mg isotope fractionation by different marine species. If the isotopic fractionations measured experimentally represent equilibrium, the wide range measured for biologically-produced carbonates demonstrate extremely large "vital" effects for Mg isotopes.

Acknowledgment

We thank Dr. Andrew Czaja for discussion on taxonomy of marine species. Prof. Huifang Xu provided Hawaiian seawater. This paper benefited from constructive comments from A. Immenhauser, E. Tipper, and M. Fantle, as well as editorial comments by G. Henderson. This study was supported by the NASA Astrobiology Institute.

Appendix A. Supplementary material

Supplementary data associated with this article can be found in the online version at http://dx.doi.org/10.1016/j.epsl.2012.04.010.

References

Albarède, F., Beard, B., 2004. Analytical methods for non-traditional isotopes, geochemistry of non-traditional stable isotopes. Mineral. Soc. Am. Washington, 113–152.
Beard, B.L., Handler, R.M., Scherer, M.M., Wu, L., Czaja, A.D., Heimann, A., Johnson, C.M., 2010. Iron isotope fractionation between aqueous ferrous iron and goethite. Earth Planet. Sci. Lett. 295, 241–250.
Bischoff, W.D., Bishop, F.C., Mackenzie, F.T., 1983. Biogenically produced magnesian calcite; inhomogeneities in chemical and physical properties; comparison with synthetic phases. Am. Mineral. 68, 1183–1188.
Black, J.R., Epstein, E., Rains, W.D., Yin, Q.-z., Casey, W.H., 2008. Magnesium-isotope fractionation during plant growth. Environ. Sci. Technol. 42, 7831–7836.
Black, J.R., Yin, Q.-z., Casey, W.H., 2006. An experimental study of magnesium-isotope fractionation in chlorophyll-*a* photosynthesis. Geochim. Cosmochim. Acta 70, 4072–4079.
Black, J.R., Yin, Q.-z., Rustad, J.R., Casey, W.H., 2007. Magnesium isotopic equilibrium in chlorophylls. J. Am. Chem. Soc. 129, 8690–8691.
Bolou-Bi, E.B., Poszwa, A., Leyval, C., Vigier, N., 2010. Experimental determination of magnesium isotope fractionation during higher plant growth. Geochim. Cosmochim. Acta 74, 2523–2537.
Brenot, A., Cloquet, C., Vigier, N., Carignan, J., France-Lanord, C., 2008. Magnesium isotope systematics of the lithologically varied Moselle river basin, France. Geochim. Cosmochim. Acta 72, 5070–5089.
Buhl, D., Immenhauser, A., Smeulders, G., Kabiri, L., Richter, D.K., 2007. Time series Δ^{26}Mg analysis in speleothem calcite: kinetic versus equilibrium fractionation, comparison with other proxies and implications for palaeoclimate research. Chem. Geol. 244, 715–729.
Chakrabarti, R., Jacobsen, S.B., 2010. The isotopic composition of magnesium in the inner Solar System. Earth Planet. Sci. Lett. 293, 349–358.

Chang, V.T.C., Makishima, A., Belshaw, N.S., O'Nions, R.K., 2003. Purification of Mg from low-Mg biogenic carbonates for isotope ratio determination using multiple collector ICP-MS. J. Anal. At. Spectrom. 18, 296–301.

Chang, V.T.C., Williams, R.J.P., Makishima, A., Belshawl, N.S., O'Nions, R.K., 2004. Mg and Ca isotope fractionation during $CaCO_3$ biomineralisation. Biochem. Biophys. Res. Commun. 323, 79–85.

Dauphas, N., Teng, F.-Z., Arndt, N.T., 2010. Magnesium and iron isotopes in 2.7 Ga Alexo komatiites: mantle signatures, no evidence for Soret diffusion, and identification of diffusive transport in zoned olivine. Geochim. Cosmochim. Acta 74, 3274–3291.

De La Rocha, C.L., DePaolo, D.J., 2000. Isotopic evidence for variations in the marine calcium cycle over the cenozoic. Science 289, 1176–1178.

de Villiers, S., Dickson, J.A.D., Ellam, R.M., 2005. The composition of the continental river weathering flux deduced from seawater Mg isotopes. Chem. Geol. 216, 133–142.

de Villiers, S., Nelson, B.K., Chivas, A.R., 1995. Biological controls on coral Sr/Ca and $\delta^{18}O$ reconstructions of sea surface temperatures. Science 269, 1247–1249.

Eisenhauer, A., Kisakurek, B., Bohm, F., 2009. Marine calcification: an alkali earth metal isotope perspective. Elements 5, 365–368.

Emiliani, C., 1955. Pleistocene temperatures. J. Geol. 63, 538–578.

Fairchild, I.J., Treble, P.C., 2009. Trace elements in speleothems as recorders of environmental change. Quat. Sci. Rev. 28, 449–468.

Fantle, M.S., DePaolo, D.J., 2007. Ca isotopes in carbonate sediment and pore fluid from ODP Site 807A: the Ca^{2+}(aq)-calcite equilibrium fractionation factor and calcite recrystallization rates in Pleistocene sediments. Geochim. Cosmochim. Acta 71, 2524–2546.

Farkas, J., Bohm, F., Wallmann, K., Blenkinsop, J., Eisenhauer, A., van Geldern, R., Munnecke, A., Voigt, S., Veizer, J., 2007a. Calcium isotope record of Phanerozoic oceans: implications for chemical evolution of seawater and its causative mechanisms. Geochim. Cosmochim. Acta 71, 5117–5134.

Farkas, J., Buhl, D., Blenkinsop, J., Veizer, J., 2007b. Evolution of the oceanic calcium cycle during the late Mesozoic: evidence from $\delta^{44/40}Ca$ of marine skeletal carbonates. Earth Planet. Sci. Lett. 253, 96–111.

Galy, A., Bar-Matthews, M., Halicz, L., O'Nions, R.K., 2002. Mg isotopic composition of carbonate: insight from speleothem formation. Earth Planet. Sci. Lett. 201, 105–115.

Galy, A., Yoffe, O., Janney, P.E., Williams, R.W., Cloquet, C., Alard, O., Halicz, L., Wadhwa, M., Hutcheon, I.D., Ramon, E., Carignan, J., 2003. Magnesium isotope heterogeneity of the isotopic standard SRM980 and new reference materials for magnesium-isotope-ratio measurements. J. Anal. At. Spectrom. 18, 1352–1356.

Handler, M.R., Baker, J.A., Schiller, M., Bennett, V.C., Yaxley, G.M., 2009. Magnesium stable isotope composition of Earth's upper mantle. Earth Planet. Sci. Lett. 282, 306–313.

Hays, J.D., Imbrie, J., Shackleton, N.J., 1976. Variations in the earth's orbit: pacemaker of the ice ages. Science 194, 1121–1132.

Heuser, A., Eisenhauer, A., Bohm, F., Wallmann, K., Gussone, N., Pearson, P.N., Nagler, T.F., Dullo, W.-C., 2005. Calcium isotope ($\delta^{44/40}Ca$) variations of Neogene planktonic foraminifera. Paleoceanography 20, PA2013.

Higgins, J.A., Schrag, D.P., 2010. Constraining magnesium cycling in marine sediments using magnesium isotopes. Geochim. Cosmochim. Acta 74, 5039–5053.

Hippler, D., Buhl, D., Witbaard, R., Richter, D.K., Immenhauser, A., 2009. Towards a better understanding of magnesium-isotope ratios from marine skeletal carbonates. Geochim. Cosmochim. Acta 73, 6134–6146.

Huang, F., Glessner, J., Ianno, A., Lundstrom, C., Zhang, Z., 2009. Magnesium isotopic composition of igneous rock standards measured by MC-ICP-MS. Chem. Geol. 268, 15–23.

Immenhauser, A., Buhl, D., Richter, D., Niedermayr, A., Riechelmann, D., Dietzel, M., Schulte, U., 2010. Magnesium-isotope fractionation during low-Mg calcite precipitation in a limestone cave—field study and experiments. Geochim. Cosmochim. Acta 74, 4346–4364.

Jacobson, A.D., Zhang, Z., Lundstrom, C., Huang, F., 2010. Behavior of Mg isotopes during dedolomitization in the Madison Aquifer, South Dakota. Earth Planet. Sci. Lett. 297, 446–452.

Jimenez-Lopez, C., Romanek, C.S., Caballero, E., 2006. Carbon isotope fractionation in synthetic magnesian calcite. Geochim. Cosmochim. Acta 70, 1163–1171.

Jimenez-Lopez, C., Romanek, C.S., Huertas, F.J., Ohmoto, H., Caballero, E., 2004. Oxygen isotope fractionation in synthetic magnesian calcite. Geochim. Cosmochim. Acta 68, 3367–3377.

Kim, S.-T., O'Neil, J.R., 1997. Equilibrium and nonequilibrium oxygen isotope effects in synthetic carbonates. Geochim. Cosmochim. Acta 61, 3461–3475.

Kim, S.-T., Hillaire-Marcel, C., Mucci, A., 2006. Mechanisms of equilibrium and kinetic oxygen isotope effects in synthetic aragonite at 25 °C. Geochim. Cosmochim. Acta 70, 5790–5801.

Kisakurek, B., Niedermayr, A., Moeller, M.N., Taubner, I., Eisenhauer, A., Dietzel, M., Buhl, D., Fietzke, J., Erez, J., 2009. Magnesium isotope fractionation in inorganic and biogenic calcite. Geochim. Cosmochim. Acta 73, A663.

Lea, D.W., 2003. Elemental and isotopic proxies of past ocean temperatures. In: Elderfield, H. (Ed.), The Oceans and Marine Geochemistry. Elsevier, New York, pp. 365–390.

Lemarchand, D., Wasserburg, G.J., Papanastassiou, D.A., 2004. Rate-controlled calcium isotope fractionation in synthetic calcite. Geochim. Cosmochim. Acta 68, 4665–4678.

Li, W.-Y., Teng, F.-Z., Ke, S., Rudnick, R.L., Gao, S., Wu, F.-Y., Chappell, B.W., 2010. Heterogeneous magnesium isotopic composition of the upper continental crust. Geochim. Cosmochim. Acta 74, 6867–6884.

Li, W., Beard, B.L., Johnson, C.M., 2011. Exchange and fractionation of Mg isotopes between epsomite and saturated $MgSO_4$ solution. Geochim. Cosmochim. Acta 75, 1814–1828.

Ling, M.-X., Sedaghatpour, F., Teng, F.-Z., Hays, P.D., Strauss, J., Sun, W., 2011. Homogeneous magnesium isotopic composition of seawater: an excellent geostandard for Mg isotope analysis. Rapid Commun. Mass Spectrom. 25, 2828–2836.

Liu, S.-A., Teng, F.-Z., He, Y., Ke, S., Li, S., 2010. Investigation of magnesium isotope fractionation during granite differentiation: Implication for Mg isotopic composition of the continental crust. Earth Planet. Sci. Lett. 297, 646–654.

Ludwig, K.R., 1999. Using Isoplot/Ex, Version 2.01: A Geochronological Toolkit for Microsoft Excel. Berkeley Geochronology Center Special Publication, vol. 1a, pp. 1–47.

McConnaughey, T., 1989a. ^{13}C and ^{18}O isotopic disequilibrium in biological carbonates: I. Patterns. Geochim. Cosmochim. Acta 53, 151–162.

McConnaughey, T., 1989b. ^{13}C and ^{18}O isotopic disequilibrium in biological carbonates: II. In vitro simulation of kinetic isotope effects. Geochim. Cosmochim. Acta 53, 163–171.

McDermott, F., 2004. Palaeo-climate reconstruction from stable isotope variations in speleothems: a review. Quat. Sci. Rev. 23, 901–918.

Müller, M.N., Kisakürek, B., Buhl, D., Gutperlet, R., Kolevica, A., Riebesell, U., Stoll, H., Eisenhauer, A., 2011. Response of the coccolithophores *Emiliania huxleyi* and *Coccolithus braarudii* to changing seawater Mg^{2+} and Ca^{2+} concentrations: Mg/Ca, Sr/Ca ratios and $\delta^{44/40}Ca$, $\delta^{26/24}Mg$ of coccolith calcite. Geochim. Cosmochim. Acta 75, 2088–2102.

Mullin, J.W., 2001. Crystallization, 4th ed. Butterworth-Heinemann, Oxford.

O'Neil, J.R., 1986. Theoretical and experimental aspects of isotopic fractionation. Rev. Mineral. 16, 1–40.

Pearson, N.J., Griffin, W.L., Alard, O., O'Reilly, S.Y., 2006. The isotopic composition of magnesium in mantle olivine: records of depletion and metasomatism. Chem. Geol. 226, 115–133.

Pogge von Strandmann, P.A.E., 2008. Precise magnesium isotope measurements in core top planktic and benthic foraminifera. Geochem. Geophys. Geosyst. 9.

Pogge von Strandmann, P.A.E., Burton, K.W., James, R.H., van Calsteren, P., Gislason, S.R., Sigfusson, B., 2008a. The influence of weathering processes on riverine magnesium isotopes in a basaltic terrain. Earth Planet. Sci. Lett. 276, 187–197.

Pogge von Strandmann, P.A.E., James, R.H., van Calsteren, P., Gislason, S.R., Burton, K.W., 2008b. Lithium, magnesium and uranium isotope behaviour in the estuarine environment of basaltic islands. Earth Planet. Sci. Lett. 274, 462–471.

Ra, K., Kitagawa, H., Shiraiwa, Y., 2010. Mg isotopes in chlorophyll-*a* and coccoliths of cultured coccolithophores (*Emiliania huxleyi*) by MC-ICP-MS. Mar. Chem. 122, 130–137.

Romanek, C.S., Grossman, E.L., Morse, J.W., 1992. Carbon isotopic fractionation in synthetic aragonite and calcite: effects of temperature and precipitation rate. Geochim. Cosmochim. Acta 56, 419–430.

Rustad, J.R., Casey, W.H., Yin, Q.-Z., Bylaska, E.J., Felmy, A.R., Bogatko, S.A., Jackson, V.E., Dixon, D.A., 2010. Isotopic fractionation of Mg^{2+}(aq), Ca^{2+}(aq), and Fe^{2+}(aq) with carbonate minerals. Geochim. Cosmochim. Acta 74, 6301–6323.

Saulnier, S., Rolliin-Bard, C., Nathalie, V., Chaussidon, M., 2011. Mg isotope fractionation during calcite precipitation: an experimental study. Geophys. Res. Abstr. 13. EGU2011-4587.

Schauble, E.A., 2004. Applying stable isotope fractionation theory to new systems, geochemistry of non-traditional stable isotopes. Mineral. Soc. Am. Washington, 65–111.

Schauble, E.A., 2011. First-principles estimates of equilibrium magnesium isotope fractionation in silicate, oxide, carbonate and hexaaquamagnesium(2+) crystals. Geochim. Cosmochim. Acta 75, 844–869.

Shen, B., Jacobsen, B., Lee, C.-T.A., Yin, Q.-Z., Morton, D.M., 2009. The Mg isotopic systematics of granitoids in continental arcs and implications for the role of chemical weathering in crust formation. Proc. Natl. Acad. Sci. 106, 20652–20657.

Teng, F.-Z., Li, W.-Y., Ke, S., Marty, B., Dauphas, N., Huang, S., Wu, F.-Y., Pourmand, A., 2010. Magnesium isotopic composition of the Earth and chondrites. Geochim. Cosmochim. Acta 74, 4150–4166.

Teng, F.-Z., Wadhwa, M., Helz, R.T., 2007. Investigation of magnesium isotope fractionation during basalt differentiation: implications for a chondritic composition of the terrestrial mantle. Earth Planet. Sci. Lett. 261, 84–92.

Tipper, E.T., Galy, A., Bickle, M.J., 2006a. Riverine evidence for a fractionated reservoir of Ca and Mg on the continents: implications for the oceanic Ca cycle. Earth Planet. Sci. Lett. 247, 267–279.

Tipper, E.T., Galy, A., Bickle, M.J., 2008. Calcium and magnesium isotope systematics in rivers draining the Himalaya–Tibetan-Plateau region: lithological or fractionation control? Geochim. Cosmochim. Acta 72, 1057–1075.

Tipper, E.T., Galy, A., Gaillardet, J., Bickle, M.J., Elderfield, H., Carder, E.A., 2006b. The magnesium isotope budget of the modern ocean: constraints from riverine magnesium isotope ratios. Earth Planet. Sci. Lett. 250, 241–253.

Tipper, E.T., Gaillardet, J., Louvat, P., Capmas, F., White, A.F., 2010. Mg isotope constraints on soil pore-fluid chemistry: evidence from Santa Cruz, California. Geochim. Cosmochim. Acta 74, 3883–3896.

Wang, Y.J., Cheng, H., Edwards, R.L., An, Z.S., Wu, J.Y., Shen, C.C., Dorale, J.A., 2001. A high-resolution absolute-dated Late Pleistocene monsoon record from Hulu Cave, China. Science 294, 2345–2348.

Wiechert, U., Halliday, A.N., 2007. Non-chondritic magnesium and the origins of the inner terrestrial planets. Earth Planet. Sci. Lett. 256, 360–371.

Wimpenny, J., Burton, K.W., James, R.H., Gannoun, A., Mokadem, F., Gislason, S.R., 2011. The behaviour of magnesium and its isotopes during glacial weathering

in an ancient shield terrain in West Greenland. Earth Planet. Sci. Lett. 304, 260–269.
Wombacher, F., Eisenhauer, A., Böhm, F., Gussone, N., Kinkel, H., Lezius, J., Noé, S., Regenberg, M., Rüggeberg, A., 2006. Magnesium stable isotope compositions in biogenic $CaCO_3$. European Geoscience Union. Geophys. Res. Abstr. 8, 06353.
Wombacher, F., Eisenhauer, A., Böhm, F., Gussone, N., Regenberg, M., Dullo, W.C., Rüggeberg, A., 2011. Magnesium stable isotope fractionation in marine biogenic calcite and aragonite. Geochim. Cosmochim. Acta 75, 5797–5818.
Yang, W., Teng, F.-Z., Zhang, H.-F., 2009. Chondritic magnesium isotopic composition of the terrestrial mantle: a case study of peridotite xenoliths from the North China craton. Earth Planet. Sci. Lett. 288, 475–482.
Zhang, F., Xu, H., Konishi, H., Roden, E.E., 2010. A relationship between d104 value and composition in the calcite-disordered dolomite solid-solution series. Am. Mineral. 95, 1650–1656.